processes

MDPI

Article

Experiment and Simulation Research on Rock Damage Mechanism in Tooth Indentation

Qingliang Qi, Yingxin Yang *, Shiwei Niu, Lian Chen and Xu Chen

Department of Mechanical Engineering, School of Mechanical and Electrical Engineering, Southwest Petroleum University, Chengdu 610500, China
* Correspondence: 202099010147@swpu.edu.cn

Abstract: In the oil and gas drilling industry, cemented carbide teeth are one of the most widely used rock-breaking elements. In order to reveal the rock damage mechanism of tooth indentation, a series of tooth indentation experiments were conducted in this study, and an indentation simulation was also conducted as a supplement to the experiment. In the experiment, a new method to observe the inner damage status of the rock was put forward, i.e., utilizing the splitting action of the teeth to avoid unexpected rock damage that may affect the actual experiment results. The load-displacement curves and the damage status of the rock revealed that the wedge tooth was more efficient in fracturing and damaging the rock because the load requirement of the wedge tooth was lower, the narrow tooth crown generated larger specific stress in the rock; that rock-breaking advantage of the wedge tooth resulted from the occurrence of the compacted core and the tension stress generated by the core. According to the simulation results, the plastic strain in the intermediate area between the wedge teeth appeared more concentrated and increased faster, and the rock material beneath the wedge teeth was removed earlier than beneath the conical teeth, indicating that wedge teeth, disposed with proper spacing, can break rock more effectively than the conical teeth. The experiment and simulation results in this paper have proved the advantages of the wedge tooth in rock fracturing and damaging, which will provide technical support for the design and development for the drill bits applied in oil and gas drilling.

Keywords: rock damage; indentation experiment; wedge tooth; compacted core; PEEQ

Citation: Qi, Q.; Yang, Y.; Niu, S.; Chen, L.; Chen, X. Experiment and Simulation Research on Rock Damage Mechanism in Tooth Indentation. *Processes* **2023**, *11*, 464. https://doi.org/10.3390/pr11020464

Academic Editors: Zhiqiang Huang, Mingjiang Shi, Gang Li, Zhen Chen and Yachao Ma

Received: 23 December 2022
Revised: 13 January 2023
Accepted: 17 January 2023
Published: 3 February 2023

1. Introduction

In the oil and gas drilling industry, cemented carbide teeth are one of the most widely used rock-breaking elements. Mechanical penetration or indentation is a basic rock-fracturing mode in excavating and well drilling, thus research on the failure mechanisms of the rock under tooth penetration is significant for bit design, drilling parameter optimization and drilling efficiency improvement [1–5].

Liu H Y et al. have developed a rock-cutter interaction program (R-T2D) on the basis of RFPA software to simulate the rock-fracturing process of single-indenter and multi-indenter systems [6–8]. In the program, the initiation, propagation and intersection of the cracks inside the rock are clearly simulated and visualized. Souissi S et al. have utilized FEM and image analysis techniques to study the cracking areas and crack types in the rock under single-tooth and double-tooth indentation [9]. The results show that Mazars' damage model is relevant to simulating rock response under indentation loading and that indentation-induced rock damage is caused by extension strain development. Saksala T et al. have studied the rock fracturing process under the impact of multiple teeth with both experimental and numerical methods [10,11], and they have found the relationship between impact speed and the damage status of the rock. Shariati H et al. have studied the inelastic behavior of granite under the impact of sphere indenters and have pointed out the method of achieving the yield surface and expansion angle under

hydrostatic pressure [12]. Saadati et al. have conducted the Hopkinson bar experiments and spalling tests on the tensile strength of granite at high strain rates considering the influence from preexisting cracks [13]; the results have revealed that the tensile strength increased from 8 MPa under Q–S conditions to 19 MPa in the dynamic case. Zhang F and Shi X C et al. have researched the damage mechanism of the rock under a sphere indenter by simulating the indenting process in PFC3D software [14–16]. The simulation results have revealed that the damaged zone under the indenter was followed by nucleation of a full penny-shaped median crack. Qi L has conducted a set of two-dimensional wedge indentation tests [17] in which nondestructive detection techniques, including infrared thermography and acoustic emission, were employed to capture rock damage evolution information. Buljak V et al. have researched the assessments of elastic and plastic parameters of indentation exploiting the hole generated by hole-drilling tests, and a method of transitioning experimental data to sought parameters via inverse analyses was put forward [18]. Kalyan B et al. found the relationship between the value of the indentation hardness index and uniaxial compressive strength [19]. Kahraman S et al. have investigated the predictability of the uniaxial compressive strength and Brazilian tensile strength of rocks from the indentation hardness index obtained using a point load apparatus [20]. Haftani M et al. have revealed that the uniaxial compressive strength of rocks can be estimated reasonably well from indentation-testing small rock fragments [21].

Most of the existing studies were conducted in the form of simulation and concentrated on the fracture mechanism of the rock under the indentation of a single indenter [22,23]. For the fracturing process of the rock under the impact load from multiple indenters and indenters of different shapes, the experimental research results are still not sufficient [24,25]. Moreover, in order to clearly observe the propagation of cracks inside the rock under indentation, plate-like rock samples are usually used in most of the existing indoor experiment, i.e., the width of the rock is smaller than the width of indenter. The disadvantage of this experiment is that it ignores the constraints of the rock material around the damaged zones.

In this paper, both single- and multiple-tooth indentation experiments were conducted in an indentation load testing system wherein the indenters comprised two types of cemented carbide teeth with different crowns (wedge tooth and conical tooth), and the rock samples comprised sandstone (soft) and limestone (hard and brittle). In the experiment, the fracturing modes of the rocks under the indentations of different teeth were achieved and analyzed. Moreover, the damage mechanics of the rock near the impact pits were analyzed through numerical simulation. The experiment and simulation results are beneficial to understanding the rock-fracturing process of the drill bits with impact functions, and the research results are expected to provide technical support for the optimization of drill bits.

2. Experiment on Tooth Indentation

2.1. Preparation of Indenters

For cone bits (single-cone bit, tri-cone bit, etc.) used in oil and gas drilling engineering, the carbide conical tooth and wedge tooth are the most widely used rock-breaking elements [26,27]. Therefore, the indenters adopted in this paper were the conical tooth (as shown in Figure 1a) and wide-crown wedge tooth (as shown in Figure 1b). The diameters of both kinds of indenters were 14 mm, and their material was cemented carbide to ensure that the indenters could be approximately considered as rigid bodies during the indentation interaction process.

2.2. Preparation and Testing of Rock Samples

Aiming at conducting a set of comparison experiments, the rock samples selected were sandstone and limestone, of which the mechanical properties are quite different. In order to ensure similar mechanical properties and avoid possible effects of size, all rock samples were incised from the same large limestone and sandstone blocks and manufactured in the same size (190 mm × 150 mm × 220 mm). Moreover, the surfaces of the samples were properly polished to avoid the influence of surface roughness on the experiment results.

(a) (b)

Figure 1. Conical tooth (**a**) and wedge teeth (**b**) used in the experiment.

Because the indentation load would be greatly affected by the mechanical properties of the rock samples, property parameters including the uniaxial compressive stress, elasticity modulus, Poisson ratio, shear strength and internal friction angle etc., were tested carefully before the experiment. The tested rock samples were cored from the stones mentioned above, as shown in Figure 2, and the height-diameter ratio of the rock core was 2.0, with the diameter being 50 mm.

Figure 2. Rock cores used in property test.

Specifically, the uniaxial compressive stress, elasticity modulus and Poisson ratio etc. were tested on a uniaxial compression tester, and the shear strength and internal friction angle, etc., were tested on the shearing tester with an adjustable angle. The loading speed was set at 0.5~1.0 MPa/s in the uniaxial compression test and 0.03–0.05 MPa/s in the shearing test.

In the uniaxial compression test, the rock core was put on the base of the compression tester with the central axis of the core being perpendicular to the base plane, and the load (0.5~1.0 MPa/s) was gradually exerted on the top of the rock core with the pressure head until the rock core was damaged by the axial pressure P. It should be noted that both the upper end and lower end of the core were properly lubricated so the influence of friction could be reduced as much as possible. During the test process, both the axial deformation and radial deformation were measured by corresponding dial gauges, as shown in Figure 3a; on the other hand, in the shearing test, the rock core was put on the shearing base (half-cylinder) of the shearing tester with the central axis of the core being parallel to the cylinder axis, and the load (0.03~0.05 MPa/s) was gradually exerted on the upper side of the rock core until the rock core was damaged by the shearing load from the half-cylinder shearing head, as shown in Figure 3b. The test was repeated a plurality

of times with different shearing angles, and the normal pressure and shearing load were recorded to further calculate the normal stress σ_s and shearing stress τ_s of the rock.

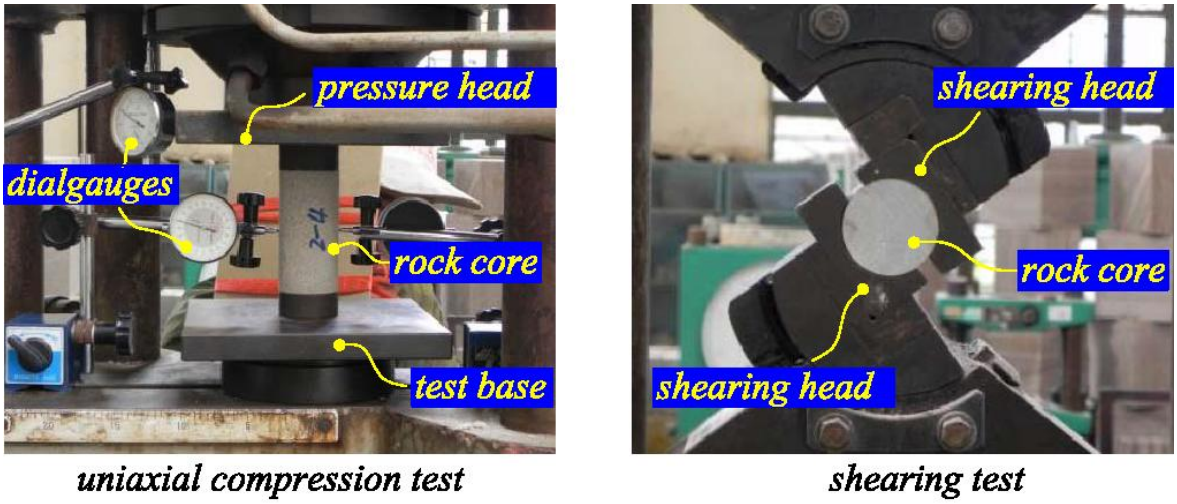

Figure 3. Uniaxial compression test (**a**) and shearing test (**b**) on the rock sample.

With the recorded data, the mechanical properties of the rock can be derived as [28]:

$$\sigma_c = P/A \tag{1}$$

where σ_c is the uniaxial compression strength, P is the axial load recorded in the uniaxial compression test and A is the cross-section area of the rock core, and:

$$E = \frac{\sigma_B - \sigma_A}{\varepsilon_{aB} - \varepsilon_{aA}} \tag{2}$$

$$\mu = \frac{\varepsilon_{rB} - \varepsilon_{rA}}{\varepsilon_{aB} - \varepsilon_{aA}} \tag{3}$$

where E is the elasticity modulus (Young's modulus), μ is the Poisson ratio, σ_A and σ_B are the normal stress values of point A and point B in the stress-strain curve (point A and point B are the start point and end point of the linear segment in the stress-strain curve of rock deformation, respectively), ε_{aA} and ε_{aB} are the axial strains of point A and B, respectively, and ε_{rA} and ε_{rB} are the radial strains of the points, respectively [29]. On the other hand, the cohesion and internal friction angle can be derived as:

$$\tau_s = C + \sigma_s \tan(\varphi) \tag{4}$$

where τ_s and σ_s are the shear stress and normal stress, respectively, calculated according to the results of the shearing test, C represents the cohesion and φ represents the internal friction angle. For the other mechanical properties, such as extension strength, hardness and drillability coefficient of these rock samples, Zhang C. has conducted relative research on them [30]; these properties are cited here in this paper. Thus, the main mechanical properties of the rock samples were achieved, as listed in Table 1.

Table 1. Main parameters of the rock samples.

Rock Sample		Sandstone	Limestone
Uniaxial compressive stress, MPa		67.548	105.951
Elasticity modulus, GPa		11.54	31.20
Poisson ratio		0.062	0.171
Extension strength, MPa		4.346	6.758
Shear strength, MPa		13.56	17.72
Hardness, MPa		1013.4	1523.6
Plasticity coefficient		2.87	1.32
Internal friction angle, °		38.03	43.62
Drillability coefficient	Cone bit	5.76	6.66
	PDC bit	5.48	7.01

2.3. Experiment Equipment and Experiment Method

A set of indentation experiment was selected to simulate the rock failure process under the indentation of both conical teeth and wedge teeth. The experiment equipment, i.e., the indentation load testing system, mainly comprised a loading system and a data acquisition system. Specifically, the loading system comprised a pressure control panel and a hydraulic pressure machine, of which the pressure was set to 0~5 t. On the other hand, the data acquisition system comprised a pressure sensor, a displacement sensor and a computer with data acquisition software.

In the experiment, as shown in Figures 4 and 5, the indenter (i.e., the cemented carbide tooth) was fixed on a tooth fixture connecting with a pressure sensor, and the pressure sensor was fixed on the movable pressure head. Meanwhile, the rock sample was fixed on the platform under the tooth. During the loading process, the tooth was lowered by the hydraulic cylinder on the upper frame of the machine. When the tooth engaged the rock, the load on the tooth and indenting displacement were collected with the pressure sensor and the displacement sensor, respectively, and then the data was further transmitted to the computer to be processed therein. In the experiment, the load was gradually increased in quasi-static mode. In order to observe the fracture behavior of the rock under different pressures, the selected loads on the sandstone were 0.3 t, 0.6 t, 0.9 t and 1.2 t, and the loads for the limestone were 0.5 t, 1 t, 1.5 t and 2.5 t. In order to avoid the influence of experimental randomness, each set of parameters was tested at least five times.

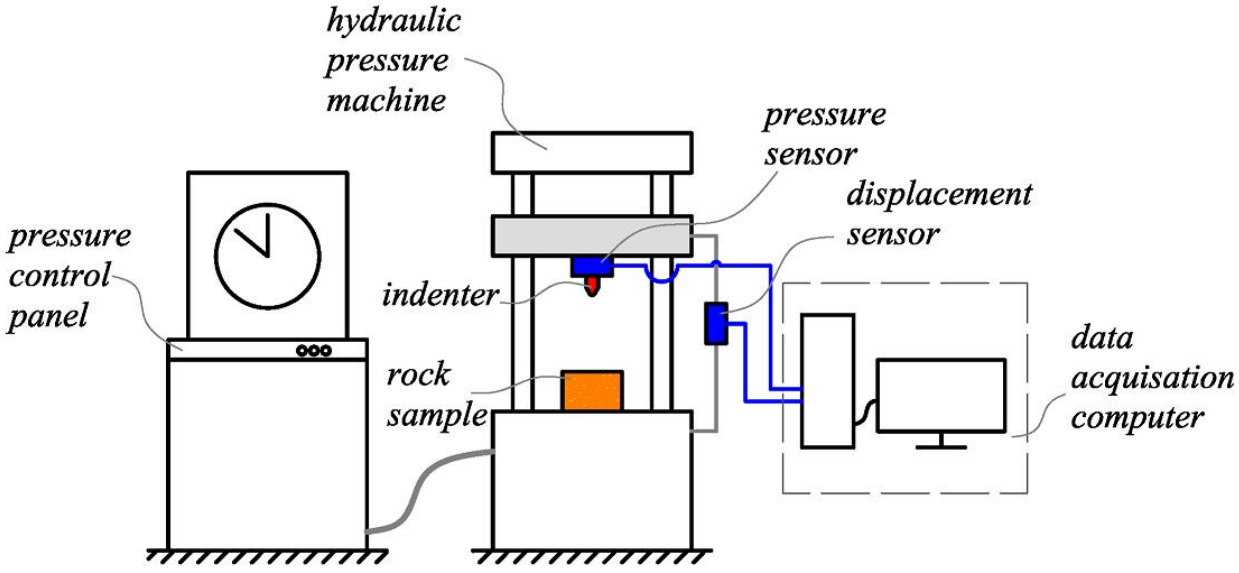

Figure 4. Schematic diagram of the indentation load testing system.

(a) (b)

Figure 5. Indentation experiment equipment (**a**) and experiment process (**b**).

During the experiment, as shown in Figure 5, it was found that the sandstone split off when the pressure was around 1.4 t whereas the limestone fractured at a load of 2.7 t, which was beneficial to the observation of the damage status inside the rock samples.

3. Experimental Analyses on the Fracture Mechanism of Indentation

3.1. Load-Displacement Relationship in Single Tooth Indentation

The load-displacement curve is a macro phenomenon that is usually used to reflect the whole process of crack initiation, propagation, intersection and macrofracture. The load-displacement curve of the conical tooth and wedge tooth indenting the sandstone and limestone are shown in Figures 6 and 7, respectively.

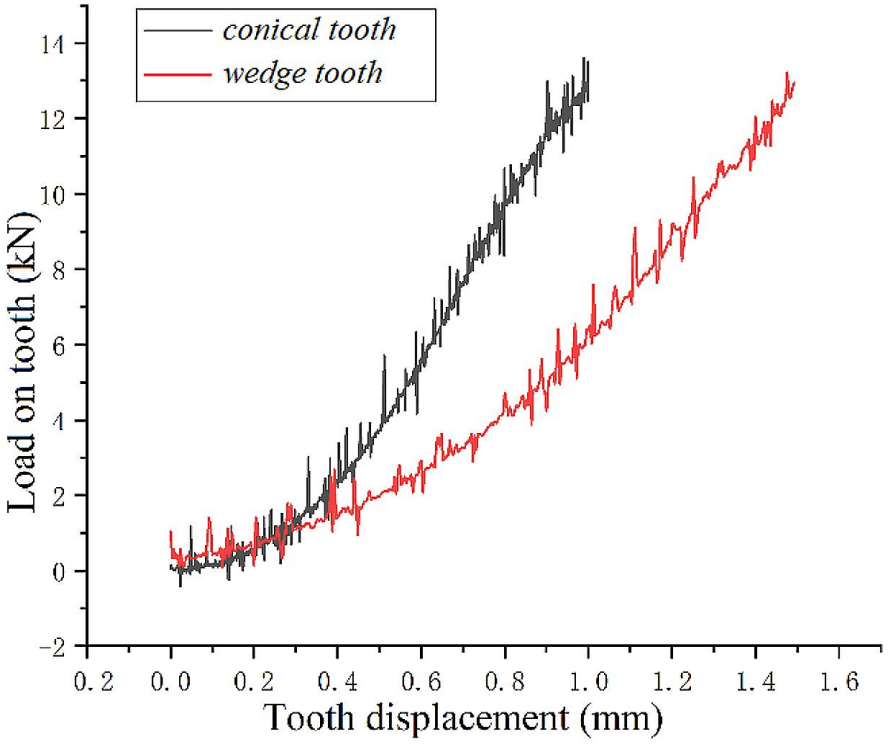

Figure 6. Load-displacement curves of the teeth indenting sandstone.

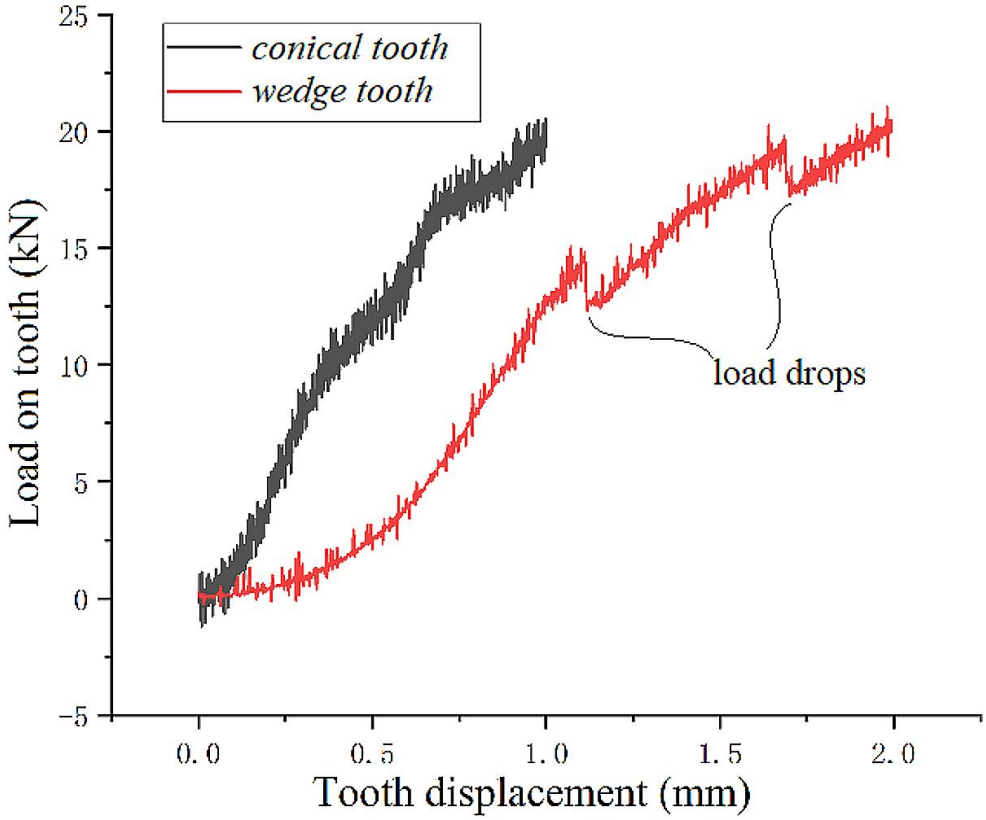

Figure 7. Load-displacement curves of the teeth indenting limestone.

Apparently, the displacement recorded in the experiment was equal to the indentation depth of the tooth. By comparing the load-displacement curves, it was found that: first, the load increased with the indentation depth, and the indentation load of the wedge tooth was apparently lower than the conical tooth with the same depth; second, for the sandstone, which is relatively soft and plastic, nearly no load drop was found in the indenting process, but only a few short cracks were observed on the rock surface, indicating that damage to the sandstone was characterized by plastic deformation. On the other hand, for hard and brittle limestone, the load drop was still not obvious in the conical tooth indentation, but was quite apparent in the wedge tooth indentation. By comparing the appearance of the rock samples, it was found that long cracks or large volumetric breakages occurred nearly every time the load dropped. The sound of rock fragmenting was also clearly heard during the experiment, indicating that the power was not absorbed by the rock but emitted in the form of crack propagation.

3.2. Fracture Characteristics on Rock Surface

Damage to the rock under the drilling of cone bits can be substantially classified into two categories, one of which is the direct volumetric breakage that formed the indentation pit on the rock surface, and the other is the cracks that formed inside the rock. Indentation pits of the conical tooth and the wedge tooth on sandstone are shown in Figures 8 and 9, respectively. It can be observed from the figures that no volumetric breakage but only indentation pits were found on the surface of the sandstone, as marked with the red circles in Figure 8, which is consistent with the smooth rising curve in the load-displacement diagram, indicating that the fracture of sandstone was mainly characterized by plastic deformation.

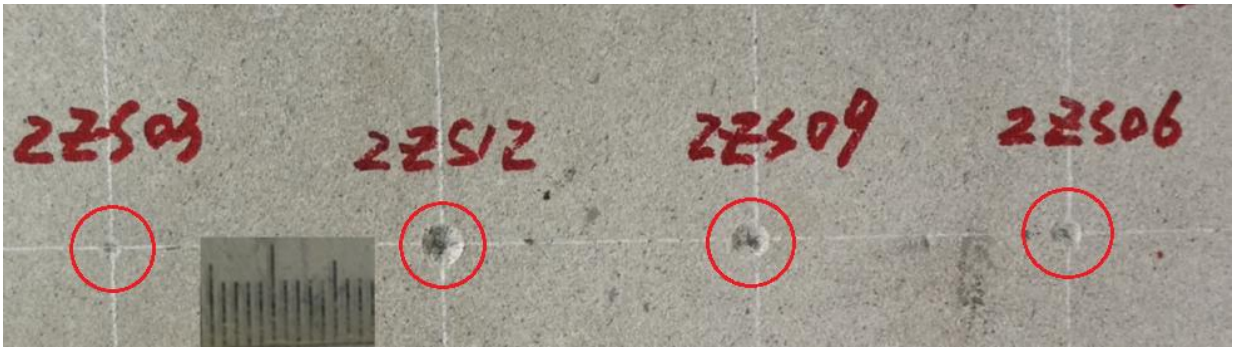

Figure 8. Indentation pits on sandstone formed by single conical tooth.

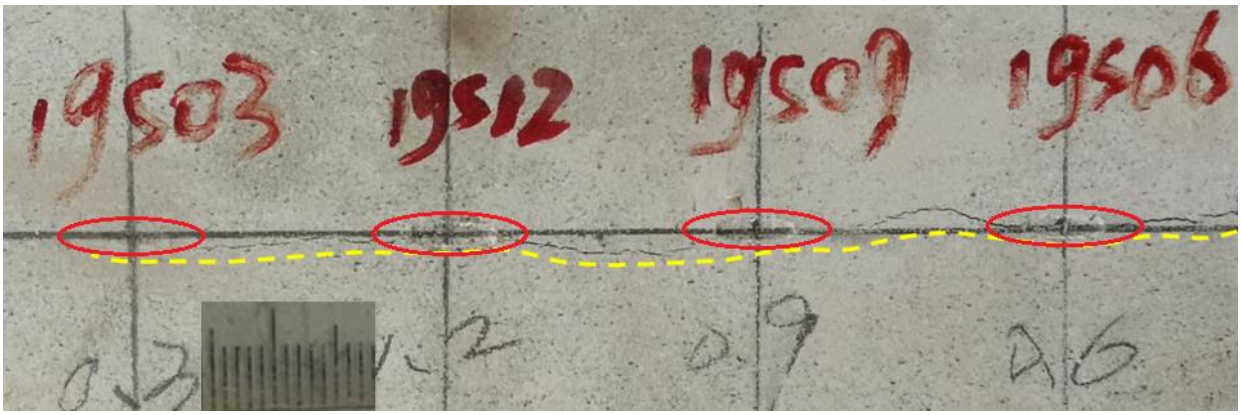

Figure 9. Indentation pits and cracks on sandstone formed by single wedge tooth.

On the other hand, interconnected cracks were found between two adjacent pits on the rock indented by the wedge tooth, as marked with the yellow dashed line in Figure 9, and that the crack direction was almost parallel to the length direction of the tooth crown, which is quite beneficial to reducing the rock's strength.

In order to further prove this phenomenon, a multiple-toothth experiment was conducted. As shown in Figure 10, wedge teeth with different mounting angles were simultaneously indented on the sandstone. Then, interconnected cracks formed in the rock as predicted as the cracks marked along the yellow dashed line in this figure, which is quite valuable for the tooth angle optimization of the bit.

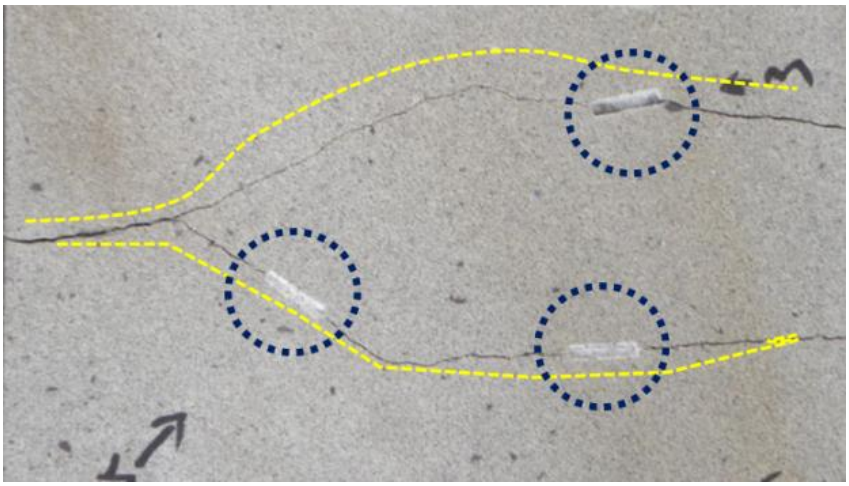

Figure 10. Indentation pits and cracks on sandstone formed by wedge tooth group.

Comparing the length and area of the pits formed by conical teeth and wedge teeth on the sandstone, as shown in Figure 11, it was found that the fracturing length increased with indentation depth, and that the length formed by the wedge teeth were larger than the conical teeth with the same load.

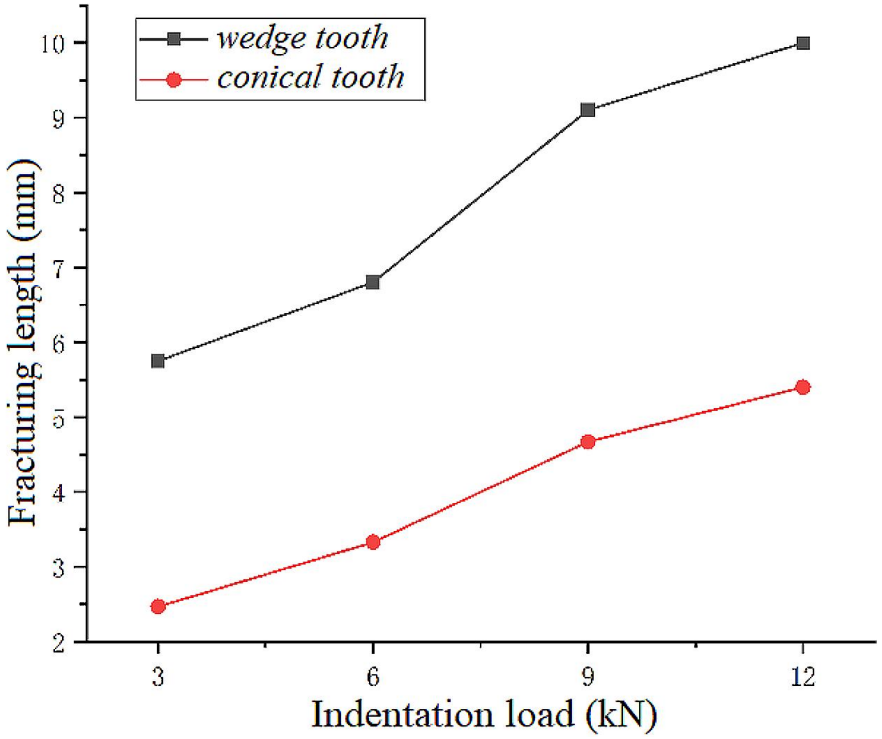

Figure 11. Fracturing length of the conical tooth and wedge tooth.

As for the limestone, the macroindenting results at a load of 1 t, 1.5 t and 2 t are shown in Figures 12 and 13 for conical and wedge teeth, respectively. The fracturing pits of the conical tooth were still round and small, and volumetric breakage could be found only when the load reached 2 t, as shown in Figure 12. By comparison, the pits formed with a wedge tooth tended to be oval and much larger, and obvious volumetric breakages could be observed when the load was just 1 t, as shown in Figure 13.

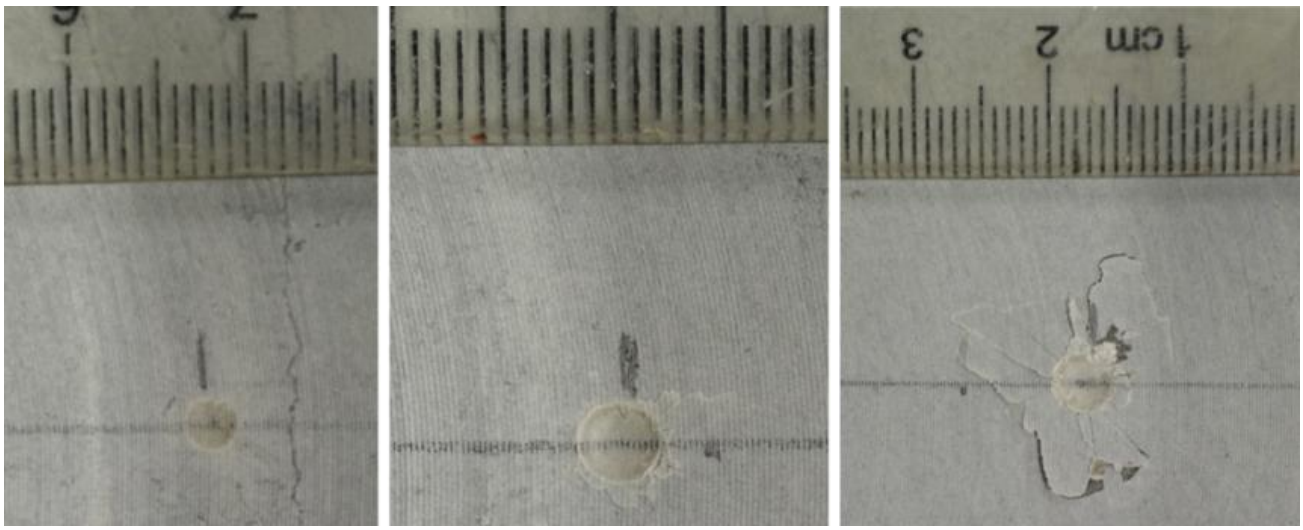

Figure 12. Indentation pits on limestone formed by conical tooth.

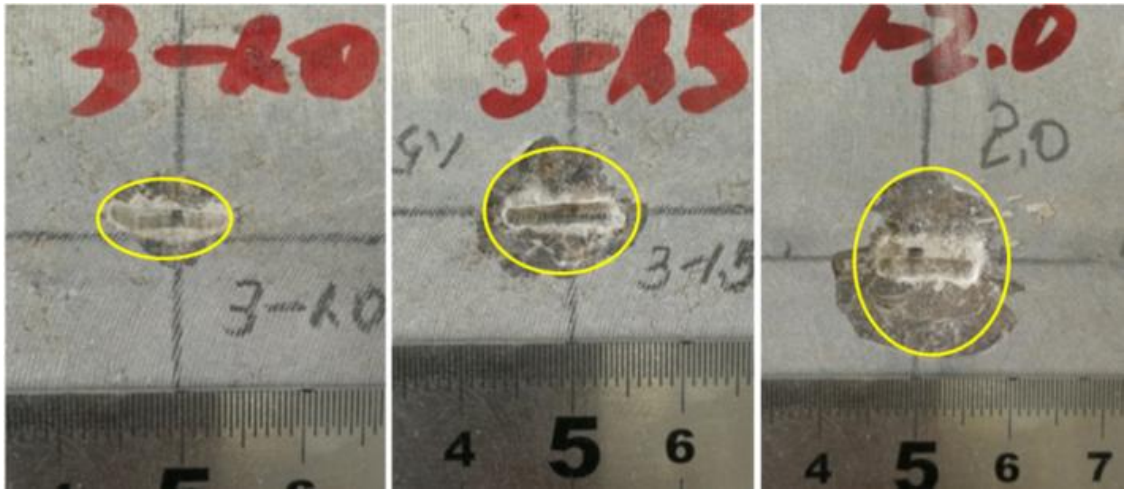

Figure 13. Indentation pits on limestone formed by wedge tooth.

When the load reacheed 1.5 t, large volumetric breakage occurred around the indenting pit of the wedge tooth, and the load curve suddenly dropped. This is because the rock under the tooth was suddenly damaged when the specific pressure reached a certain level. Thus the displacement of the tooth increased in a short amount of time, and then the tooth engaged the rock again and the load kept growing. When the load reached 2 t, as the indenting depth grew, more rock debris in powder form and large rock flakes were generated around the pits. The total fracturing area was more than 10 times that of the original indenting pit, indicating that the wedge tooth could not only lengthen the indenting pit, but could also obviously enlarge the rock-fracturing area.

When the load was lower than a certain level, neither the conical tooth nor wedge tooth generated volumetric breakage; only indenting pits were formed on the rock surface, thus the fracturing areas formed by the two teeth were nearly the same. As the load increased, the volumetric breakage formed with the wedge tooth came earlier and was much larger than that of the conical tooth, thus the fracturing area of the wedge tooth became obviously larger than that of the conical tooth, as shown in Figure 14.

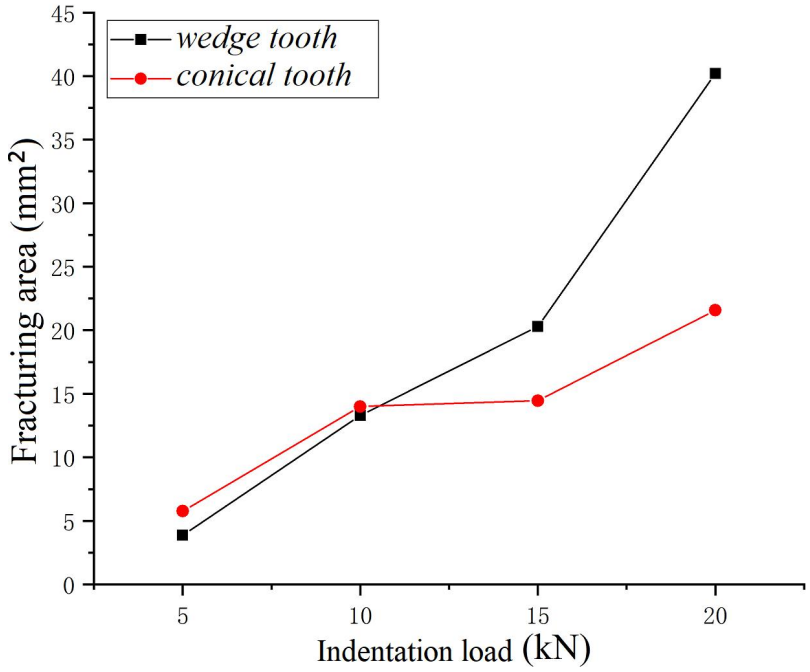

Figure 14. Fracturing areas of the conical tooth and wedge tooth.

The fracture behavior of the rock when indented by wedge tooth indicated that the fractured volumetric on the rock surface was mainly caused by the tension and shearing action of the wedge tooth. Specifically, when the wedge tooth penetrated the rock, the side faces of the tooth pushed the rock against them and generated tension or shearing stress inside the rock. Once the tension or shearing stress reached the strength limit, the rock material was then fractured and removed. For most of the rock in the bottom-hole of an oil or gas well, its compressive strength is much greater than its tension and shearing strength. Because the conical tooth breaks rock mainly by compressive stress, the wedge tooth can therefore break more rock than the conical tooth when they are indented in the rock with the same load, i.e., the rock-breaking efficiency of the wedge tooth is obviously greater than that of the conical tooth.

3.3. Damage Characteristics in the Rock

In addition to the fracture on the rock surface, damage in the rock is also an important part in the rock-breaking process of the tooth.

In order to directly observe the fracture and crack propagation behavior of the rock, researchers usually use indenters with greater thickness than the rock, as shown in Figure 15. However, because the rock in an actual situation would be much larger than the teeth, the fracture and damage behavior of the rock sample with low thickness cannot really reflect the actual rock-breaking process in the bottom-hole.

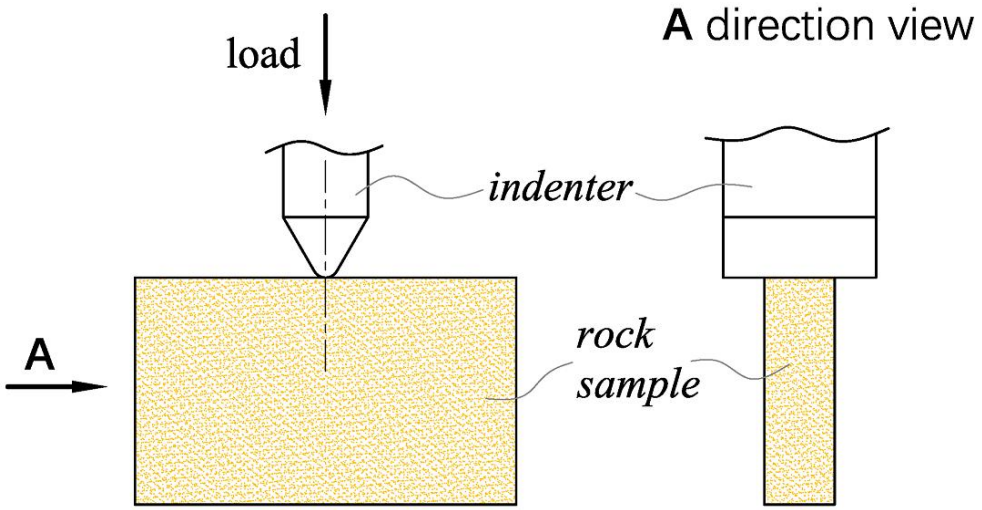

Figure 15. Indentation model of wide indenter on a thin rock sample.

Moreover, there is another method usually used to observe the rock-breaking process: when a large rock sample is fractured and damaged by indenters, the sample will be cut across the center of the indenting pit by using a cutting machine so the fractured and damage area will be exposed. However, because the cutting process will damage the indentation pits on the rock, the actual damage generated by the indenter still cannot be observed.

During the single-tooth indentation experiment, intersecting and connecting cracks were usually found in the rock. Once the main cracks intersected and connected, the rock was then split into two parts, as shown in Figure 16. This phenomenon was used to observe the fracture and damage behavior of the rock.

Figure 16. Rock sample split along connected cracks.

The cross-section view of the rock sample indented by wedge tooth is shown in Figure 17a,b. According to the pictures, there was a white area and a piece of wedge-like rock powder body on the upper surface of the area, which was the damaged area in the rock. The wedge-like rock material was substantially independent from the rock sample and was easily removed. In fact, the powder-like rock piece is called the compacted core, which is formed because the strong pressure or impact force crushed the rock. The compacted core is an important part for transmitting load in the rock, as shown in Figure 17c,d.

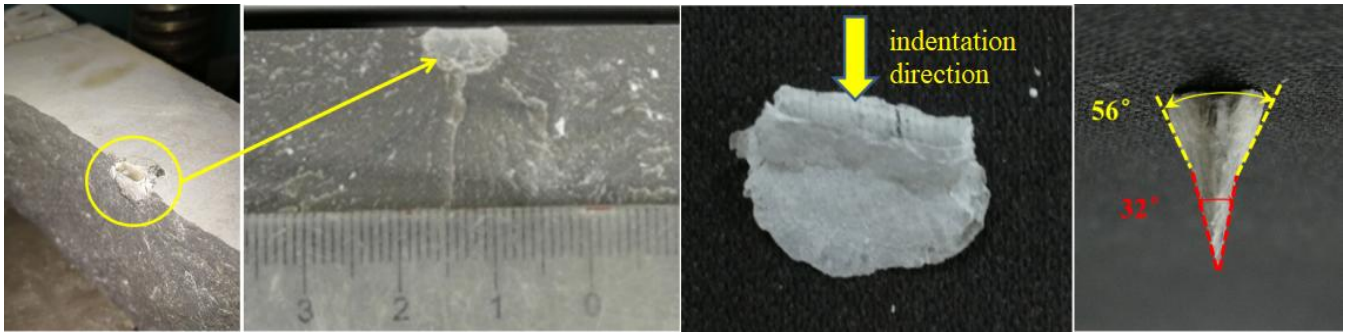

(**a**) (**b**) (**c**) (**d**)

Figure 17. Damaged area and compacted core generated with wedge tooth in the limestone ((**a**) indentation pit, (**b**) damaged area under indentation, (**c**) side view of the compacted core, (**d**) front view of the compacted core).

The damage inside the rock was caused by the compacted core continuously wedging in and pressing on the rock material with great force. The wedging or pressing force (as the force F_w shown in Figure 18) generated tension stress in the rock. Once the tension stress reached the limit of the rock's strength, the rock around the core was split, as shown in Figure 18. Therefore, the fracture of rock can be explained as the results of the wedging action of the compacted core formed with the indenter.

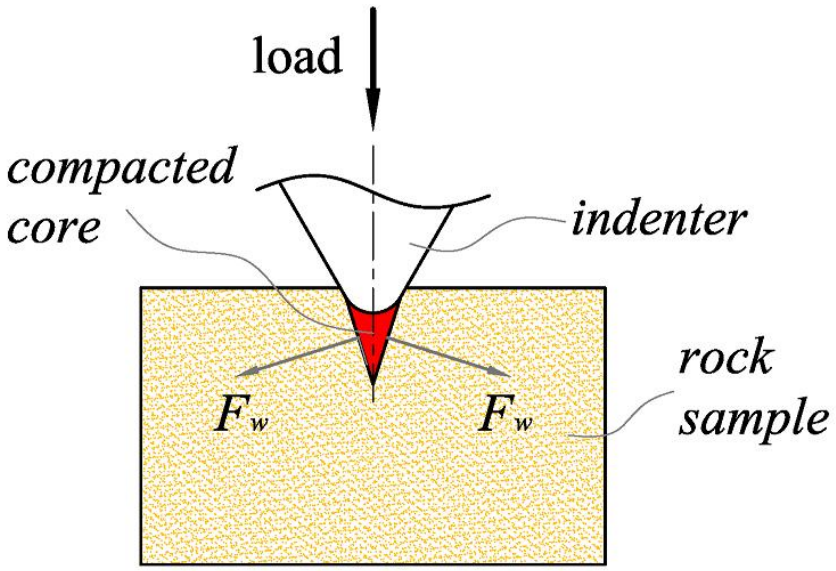

Figure 18. Wedging action of the compacted core.

Rock damage status under different indentation loads are shown in Figure 19. In these images, the white area in the split rock sample clearly represents the damage status within the rock. It can be observed that the damaged area was approximately an ellipse, of which the major axis was about 1~1.5 mm beneath the rock surface, and there were a series of radial cracks around the ellipse. Apparently, the maximum length of the damaged area was longer than the contacting length on the rock.

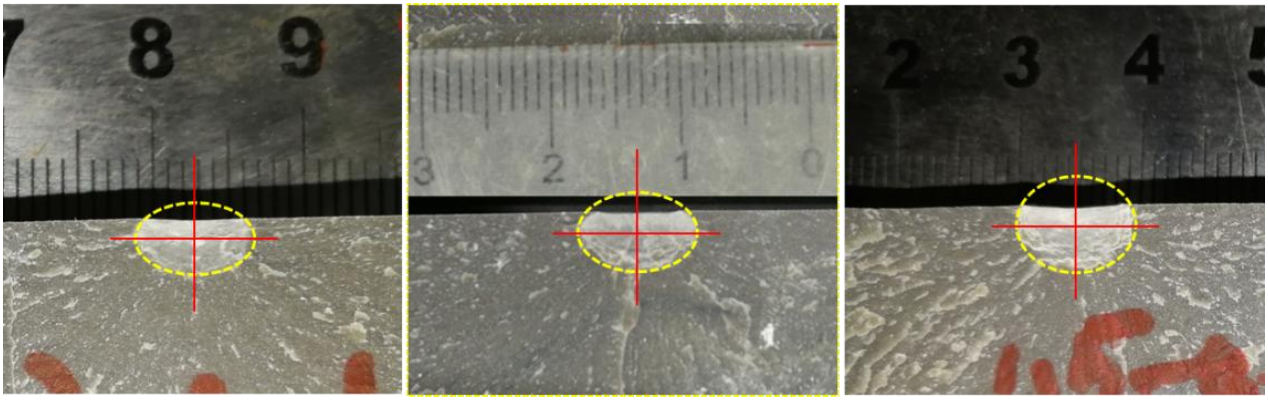

(**a**) (**b**) (**c**)

Figure 19. Damaged area in limestone generated by wedge tooth under different loads: (**a**) 1.0 t; (**b**) 1.5 t; (**c**) 2.0 t.

The variation of the major and minor axes of the damaged area generated by wedge teeth under different loads is shown in Figure 20. As the load increased, the length of the major axis increased obviously, whereas the minor axis changed a little, i.e., the indentation load affects the damage length much more than the damage depth. As the load increased, the contacting length increased simultaneously; therefore, more load was absorbed by the increased length. On a macro scale, a larger indentation load affects the length direction of the damaged area much more.

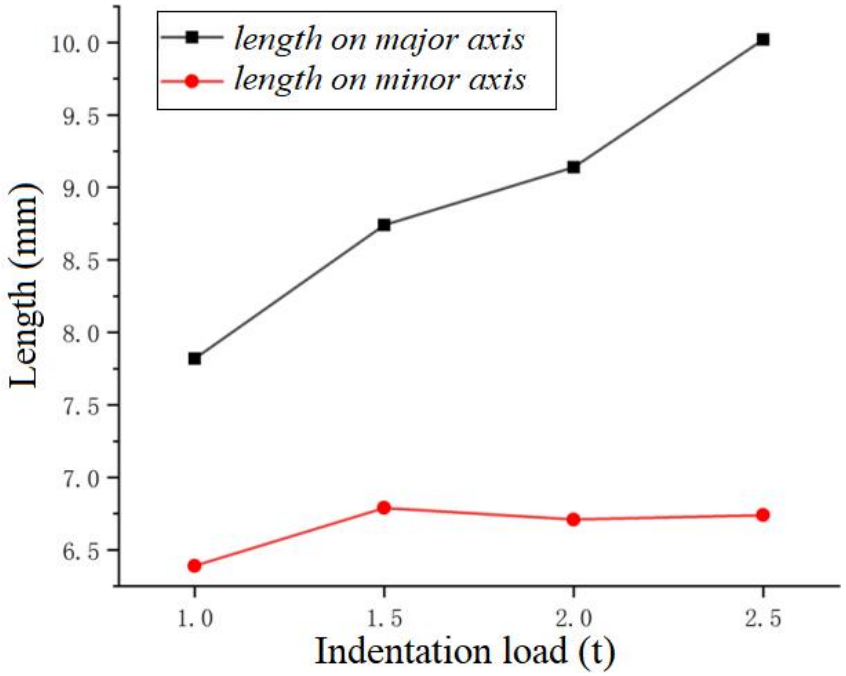

Figure 20. Length variation of major and minor axes of the damaged area.

On the other hand, the fracture and damage of the rock sample under the indentation of conical tooth was also tested, as shown in Figure 21. Similarly, there was also a compacted core in the fracture area. It should be noted that although the crown of the conical tooth was different from the wedge tooth, the lower part of the compacted core was still an ellipse; the difference is that the crack propagation direction of the conical tooth indentation was not certain like that of the wedge tooth indentation, as the crack propagation direction was affected by the original internal defects of the rock sample.

(**a**) (**b**) (**c**)

Figure 21. Damaged area and compacted core generated by conical tooth in the limestone.

As for the indentation of the wedge tooth in sandstone, the fracture status and compacted core generated under the load of 1.5 t is shown in Figure 22. It can be observed that there a compacted core formed inside the rock, and that the core also has a wedge-like body as in the limestone. The difference is that no obvious radial cracks could be found in the sandstone. This is because the sandstone is a kind of rock material with relatively higher plasticity, thus more impacting power will be absorbed by the rock material near the indentation area. Because the generation of cracks requires enough power, more power consumption means fewer cracks can be generated. This is the reason for the low drilling efficiency of the cone bits drilling in rock with high plasticity.

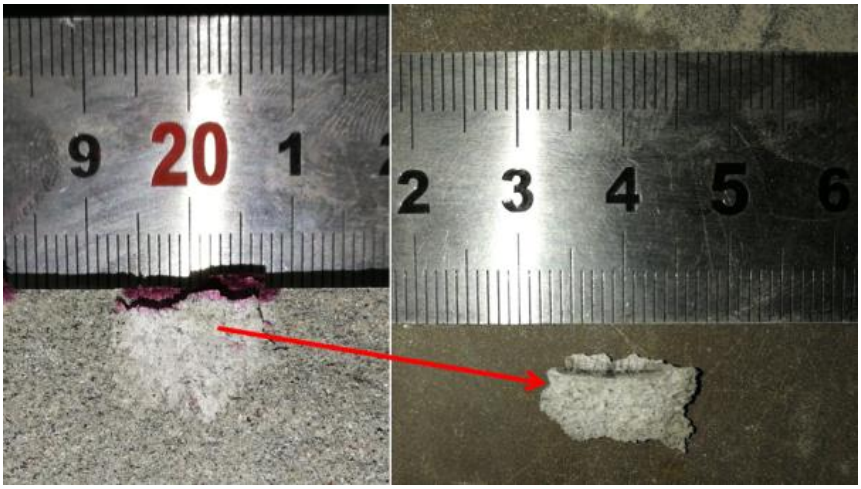

Figure 22. Damaged area generated with wedge tooth in sandstone.

3.4. Discussion of the Experiment Results

First, the load-displacement curves show that the load on the wedge tooth was obviously lower than the conical tooth with the same displacement, and that obvious load drops were observed when the wedge tooth generated volumetric rock breakage in limestone, revealing that the load requirement of the wedge tooth is lower than the conical tooth.

Second, in the indentation experiment on sandstone, nearly no volumetric rock breakage was observed, but interconnected cracks were generated by the wedge tooth. For indentation on limestone, volumetric breakage was generated by the conical tooth only if the load was large enough, but obvious volumetric breakage was generated by the wedge tooth even when the load was quite low, indicating that the wedge tooth is more efficient in fracturing and damaging the rock, especially in the limestone.

Third, damage features in the rock in the limestone revealed that the rock-breaking advantage of the wedge tooth resulted from the occurrence of a compacted core and the tension stress generated by this compacted core.

Therefore, one of the most efficient methods to generate damage in the rock is to amplify tension stress in the rock. For the roller-cone bits or hybrid PDC bits configured with roller-cones used in oil and gas drilling, the tooth should be designed with a long and sharp crown, such as the wedge tooth researched in this paper.

4. Numerical Simulations on the Tooth Indentation

4.1. Constitutive Model of Rock Material

To further study the fracture and damage status of the rock under indentation, a series of numerical simulations was conducted. Because the rock is a kind of particulate material, shearing dilatation will occur when the rock suffers from a certain level of normal stress. In the Drucker–Prager strength criterion (hereinafter referred to as the D–P criterion), both the shearing dilatation effect and the influence of principal stress on the yield characteristics of material are considered; therefore, the D–P criterion is usually applied in rock-breaking research. In the criterion, the normal stress σ_oct and shearing strength τ_oct on a regular octahedron are derived as [31]:

$$\tau_{oct} = \tau_0 + m\sigma_{oct} \tag{5}$$

$$\begin{cases} \tau_{oct} = \frac{1}{3}\sqrt{(\sigma_1-\sigma_2)^2+(\sigma_2-\sigma_3)^2+(\sigma_3-\sigma_1)^2} \\ \sigma_{oct} = \frac{1}{3}(\sigma_1+\sigma_2+\sigma_3) \\ m = -\sqrt{6}\alpha, \tau_0 = \frac{\sqrt{6}}{3}C \end{cases}, \tag{6}$$

$$\alpha = \frac{2\,sin\varphi}{\sqrt{3}(3-sin\varphi)} \tag{7}$$

$$C = \frac{6c\ cos\varphi}{\sqrt{3}(3 - sin\varphi)} \tag{8}$$

where σ_1, σ_2 and σ_3 are the principal stresses on a certain point in the rock, c represents the cohesive force, φ represents the internal friction angle and C and α are the relevant strength parameter determined with c and φ, respectively. On the other hand, the yield behavior of the material can be determined according to the yield-surface model. According to the D–P criterion, the yield curve surface applied in this paper can be represented as:

$$\begin{cases} \tau - p\ tan\varphi - C = 0 \\ \tau = \frac{1}{2}\sigma[1 + \frac{1}{k} - \left(1 - \frac{1}{k}\right)\left(\frac{r}{q}\right)^3] \end{cases} \tag{9}$$

where k is the flow stress ratio (generally, $0.778 \leq k \leq 1$), $q = \sqrt{\left(\frac{3}{2}\right)S : S}$, and S is the deviatoric stress tensor, where $S = \sigma + pI$ and p is the equivalent stress, i.e., $p = \frac{1}{3}(\sigma_x + \sigma_y + \sigma_z)$. According to the D–P criterion, the damage model of the rock material in this paper is defined as shear damage, which is a phenomenological model for predicting rock damage caused by variation of the shearing area. In the shear damage model, the PEEQ (i.e., the equivalent plastic strain) at the node of a certain integral unit is used to evaluate the damage of the material. When the PEEQ of a certain node in the material reaches the limit value, the material around this node will start to fracture and then be removed from the rock sample. In this model, the equivalent plastic strain is represented as a function of shear stress ratio and equivalent plastic strain ratio, which is:

$$\bar{\varepsilon}_s^{pl} = \left(\theta_s, \bar{\varepsilon}^{pl}\right) \tag{10}$$

where $\bar{\varepsilon}_s^{pl}$ is the equivalent plastic strain, θ_s is the shear stress ratio and $\bar{\varepsilon}^{pl}$ is the equivalent plastic strain ratio. Accordingly, the fracture condition can be derived as:

$$w_s = \int \frac{d\bar{\varepsilon}^{pl}}{\bar{\varepsilon}_s^{pl}\left(\theta_s, \bar{\varepsilon}^{pl}\right)} \tag{11}$$

where w_s is a status variable that monotonically increases with plastic strain, of which the increment is:

$$\Delta w_s = \frac{\Delta\bar{\varepsilon}^{pl}}{\bar{\varepsilon}_s^{pl}\left(\theta_s, \bar{\varepsilon}^{pl}\right)} \geq 0 \tag{12}$$

The fracture of rock is a gradual process. Before the rock material is removed, the strength of the rock will be gradually decreased. Specifically, the stress-strain variation curve of the material is shown in Figure 23, where the dashed curve represents the stress-strain relationship of the material without damage and the solid curve represents the relationship after damage. As shown in this figure, point A is the point where the rock damage starts, where the yield stress is σ_{y0} and the equivalent plastic strain is ${\bar{\varepsilon}_0}^{pl}$ (with the global damage variable D = 1). Point B is the fracture point of the rock material, where the equivalent plastic strain is $\bar{\varepsilon}_f^{pl}$ (D = 1). Because the rock material gradually fractures in the segment from point A to point B, the mechanical behavior of the material cannot be correctly reflected by the curve. Therefore, equivalent plastic displacement $\overline{u}^{pl}$ or fracture energy G_f should be introduced to describe the fracturing process of the material. In this paper, the equivalent plastic displacement $\overline{u}^{pl}$ of the material was applied to define the fracturing of rock material, i.e., the fracture condition of the rock is:

$$\dot{\overline{u}}^{pl} = L\dot{\bar{\varepsilon}}^{pl} \tag{13}$$

where $\dot{\overline{u}}^{pl}$ is defined as the fracture status variable and as the differential of $\overline{u}^{pl}$, and it is further simplified as $d = \dot{\overline{u}}^{pl} = d\left(\overline{u}^{pl}\right)$. Specifically, when the rock material is fractured, the equivalent plastic displacement is ${\overline{u}_f}^{pl}$. Further, the variation of the fracture status variable follows the equation below. If $\overline{u}^{pl} = {\overline{u}_f}^{pl}$, then d = 1, i.e., the strength of material decreases to its minimum value, and at this point, the material is fractured.

$$\dot{d} = \frac{L\dot{\overline{\varepsilon}}^{pl}}{{\overline{u}_f}^{pl}} = \frac{\dot{\overline{u}}^{pl}}{{\overline{u}_f}^{pl}} \tag{14}$$

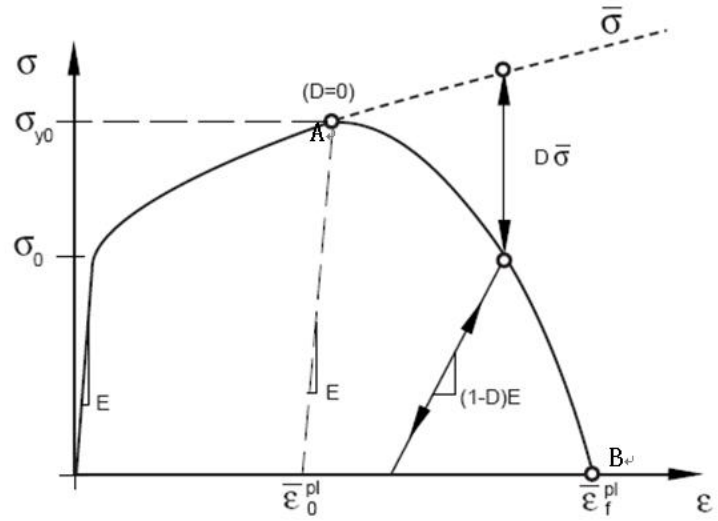

Figure 23. Stress-strain curve of the material.

4.2. Simulation Method and Process

In accordance with the experiment, the mechanical properties (as listed in Table 1) of limestone were used as the constitutive parameters in the simulation. In fact, the mechanical properties applied in this paper are measured with a physical method, but inverse analysis on the constitutive parameters should be conducted to achieve precise simulation results, and many researchers have put forward a series of methods for parameter identification [32]. However, the simulation in this paper is to find out the strain trend in the rock model and strain differences between the rock models indented by wedge tooth and conical tooth. Therefore, constitutive parameters applied in this paper were achieved from traditional tests. Moreover, as a supplementary support for the indentation experiment, the equivalent plastic strain was introduced to describe the deformation of the rock material under indentation. For detailed rock behavior during the indentation test, such as crack propagation in the rock model, further study on the simulation should be conducted [33,34].

In order to observe the damage status of the rock at a micro level, the indentation process was simulated with the finite element method by utilizing the ABAQUS software. As shown in Figure 24, in consideration of the symmetry of the model and calculation amount of the process, the symmetric model was simplified with a quarter part to improve computing efficiency. Specifically, the size of rock sample was 50 mm × 50 mm × 20 mm, and the rock model was discretized with a C3D8R unit. The indenter models were a 14 mm wedge tooth and a 14 mm conical tooth. Because the shapes of the teeth were not regular, they were discretized with a C3D10M unit. A fixed constraint was imposed on the bottom, and a symmetry constraint was imposed on the symmetry plane of the rock model. The indentation speed of the teeth was 200 mm/s, and the total time of the simulation process was 0.01 s. The minimum distance of the two adjacent teeth was 2 mm.

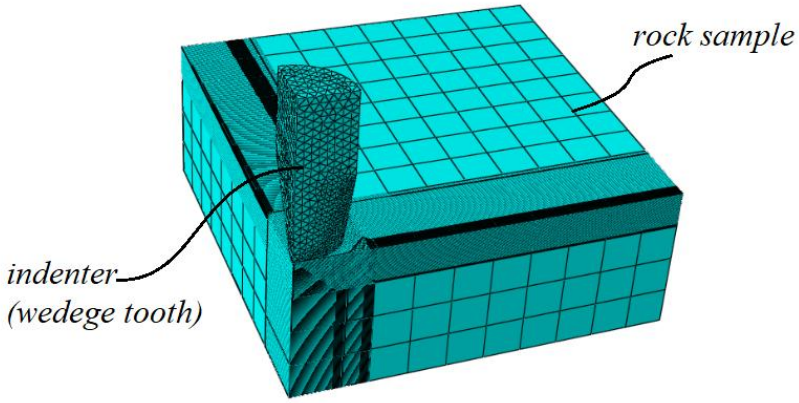

Figure 24. Indentation model in the simulation.

4.3. Analysis on the Strain of Rock

The rock-breaking performance and service life of the drill bit are directly determined by the fracture status and damage area of the rock. On the other hand, the plastic strain is a permanent strain in the deformation process of material. Thus, the plastic strain of the rock model can be used to reflect the damage condition of the rock material. In numerical simulation, PEEQ (i.e., the equivalent plastic strain as mentioned above) is an accumulation of strain in the deformation process. A PEEQ value larger than zero means the material has yielded. In order to reveal the damage status of the rock under indentation, three sets of nodes along different directions were selected to find out the strain conditions in the rock model. Specifically, the directions including the indentation direction (direction along the indentation force), the length direction (direction along the length of the wedge tooth crown) and the breadth direction (direction along the breadth of the wedge tooth crown) were used, as shown in Figure 25.

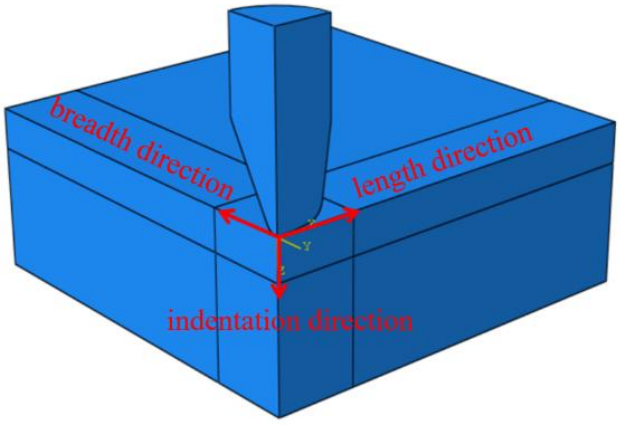

Figure 25. Directions of the selected nodes.

The strain status along the indentation direction with an indentation depth of 0.5 mm is shown in Figure 26. It should be noted that the PEEQ generated by two different teeth follows the same rule: the PEEQ first increases from the center to the edge of the contacted area when the depth is relatively small, and then it gradually decreases when the depth reaches a certain value until the PEEQ drops back to zero. According to the definition of PEEQ, the depth where PEEQ is larger than zero could be defined as the effective damage area. Obviously, the yielding or damaging degree generated by the wedge tooth was much higher than the conical tooth when the depth was smaller than 1 mm, whereas it was lower when the depth was larger than 1 mm. This phenomenon reveals that the wedge tooth with a narrower crown is better at damaging the rock material near the surface, whereas

the conical tooth is stronger in deeper rock because a narrower tooth crown can generate more stress concentration in rock material near the surface.

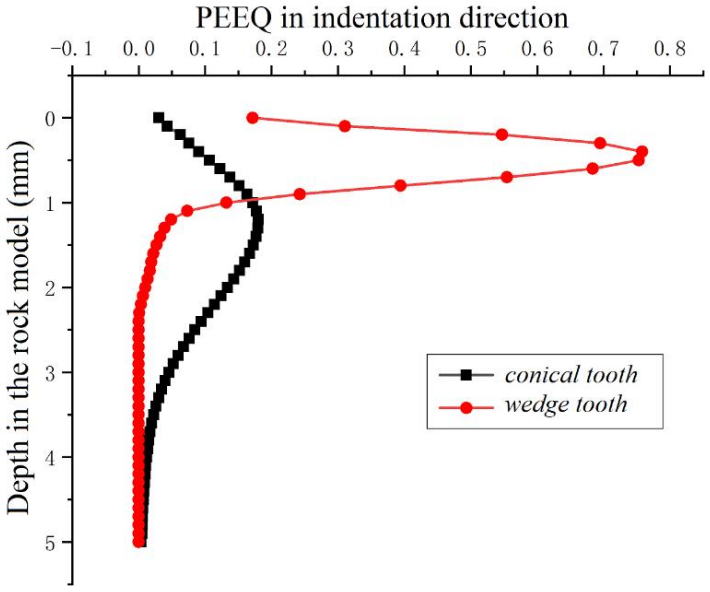

Figure 26. PEEQ of the nodes along indentation direction.

For the strain status along the length direction (when the indentation depth is 0.5 mm), the simulation results are shown in Figure 27. Obviously, the PEEQ was the largest when the nodes were close to the edge of the contacted area, which means the degree of rock damage near the edge of the contacted area was much larger than the area underneath the tooth crown. On the other hand, the damage length of the wedge tooth was about 1.6 times that of the conical tooth, thus indicating that the damage area of the wedge tooth was larger than the conical tooth.

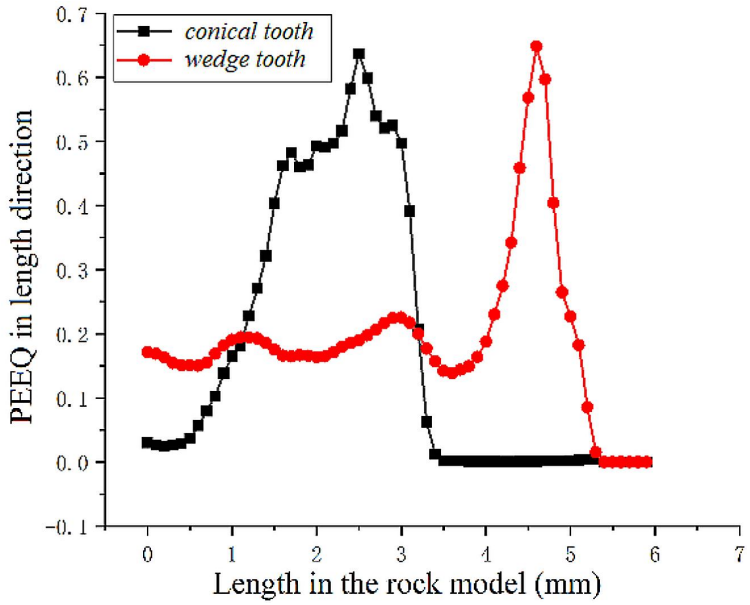

Figure 27. PEEQ of the nodes along the length direction.

For the strain status along the breadth direction (with the indentation depth being 0.5 mm), the simulation results are shown in Figure 28a. Because the conical tooth is an axisymmetric body, the strain status in its breadth direction was the same as that in its length direction. In the breadth direction, the largest PEEQ generated with the wedge

tooth was larger than the conical tooth. Under the indentation of wedge tooth, the strain suddenly dropped to zero in the area underneath the wedge tooth crown; this is because volumetric rock breaking occurs in this area, as shown in Figure 28b, which is in good accordance with the experiment results. Moreover, it can be observed that the yielding widths along the breadth direction of both teeth are nearly the same, indicating that the narrower crown of the wedge tooth did not narrow the damaging area.

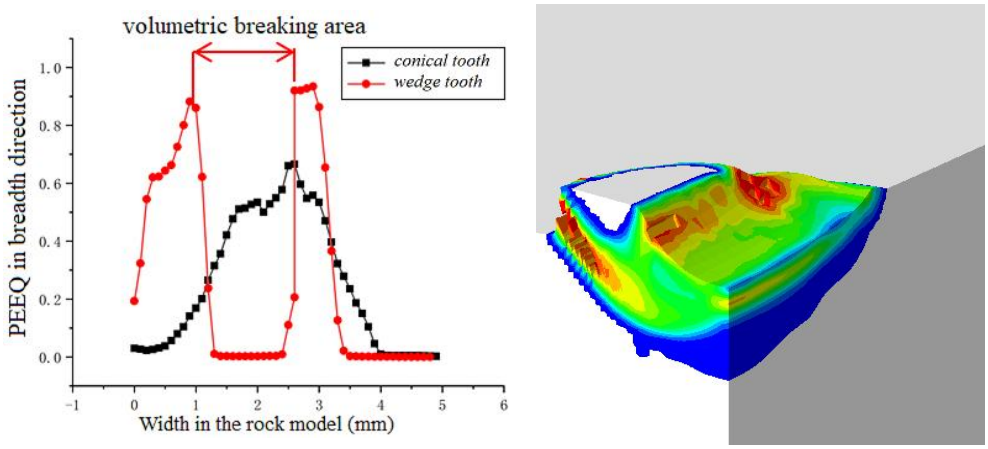

(**a**) (**b**)

Figure 28. PEEQ of the nodes along the breadth direction (**a**) and volumetric breakage (**b**).

4.4. Rock Damage between Adjacent Indenting Pits

In a roller-cone bit or roller-cone hybrid PDC bit, the teeth on the cone mainly break the rock material by indenting in the rock and forming rugged rock pits, and if the pits are close enough, rock damage will be generated between adjacent pits, which is a pre-damage process for successive teeth or fixed cutters. For the rock material that has not been directly indented but has been damaged, the strain status should be further researched.

In order to find out the strain status of the intermediate area on the rock between two adjacent indentations of the teeth, simulations on the indentation of two adjacent teeth were conducted. As shown in Figure 29, the indenters applied in the simulations included conical teeth and wedge teeth. It can be observed in the figure that plastic strain occurred both in the indentations of the conical teeth and those of the wedge teeth, and that the unbroken area between the wedge teeth was obviously smaller than that between conical teeth although the teeth spacings of the adjacent teeth were the same. Moreover, the plastic strain in the intermediate area between the wedge teeth was more concentrated than that between the conical teeth because its area was smaller and the PEEQ value was larger. This phenomenon may not be directly observable from the static picture in Figure 29, but it can be revealed from Figure 28 in the following content.

For the rock material, the damage correlated with the plastic strain. To further study damage status in the intermediate area, finite elements of the same number in the intermediate area were selected from both of the simulations. As the indentation depth increased, the PEEQ values of different elements grew differently, as shown in Figure 30. When the indentation depth was 0~2 mm, both values stayed at zero, indicating that no plastic strain occurred in either of the elements. As the depth increased, the PEEQ values of both of the elements gradually increased with it, indicating that plastic strain occurred and grew. However, the PEEQ of the element from the wedge indentation increased much faster than the cone indentation, revealing that the plastic strain on the intermediate area of wedge teeth indentation was much larger than that of the conical teeth even though the indentation depths were the same. When the depth increased to a certain level, about 0.6 mm for the wedge teeth and 1.0 mm for the conical teeth, the PEEQ at the intermediate area stopped increasing. This is because the stress on the finite elements beneath the tooth crown have exceeded its limits, thus the elements were eliminated and the stress around

this area was released. Otherwise, the PEEQ that resulted from wedge teeth indentation would still be growing.

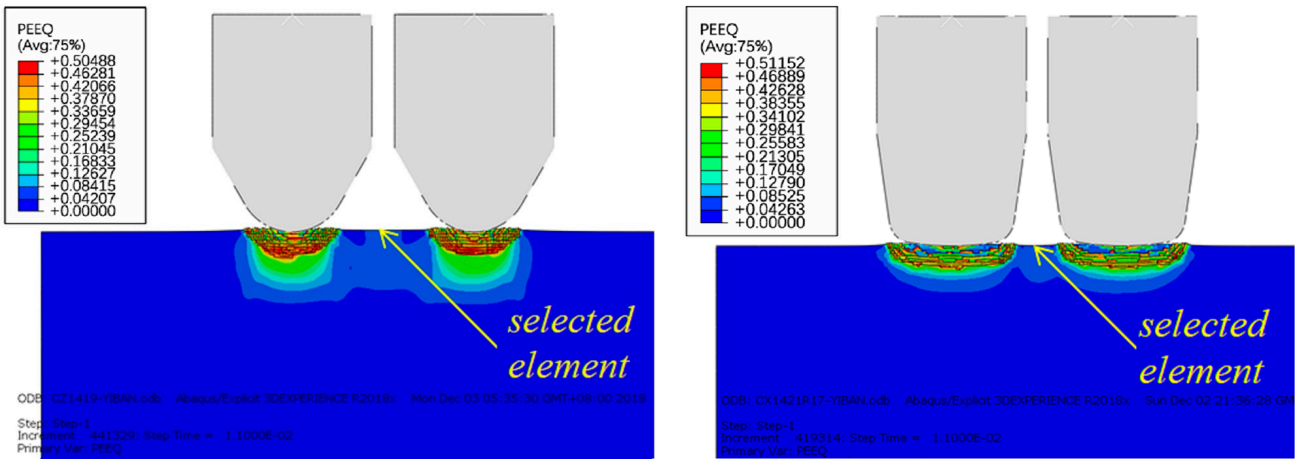

(**a**) (**b**)

Figure 29. Rock damage and strain status in double-teeth indentation: (**a**) conical teeth indentation; (**b**) wedge teeth indentation.

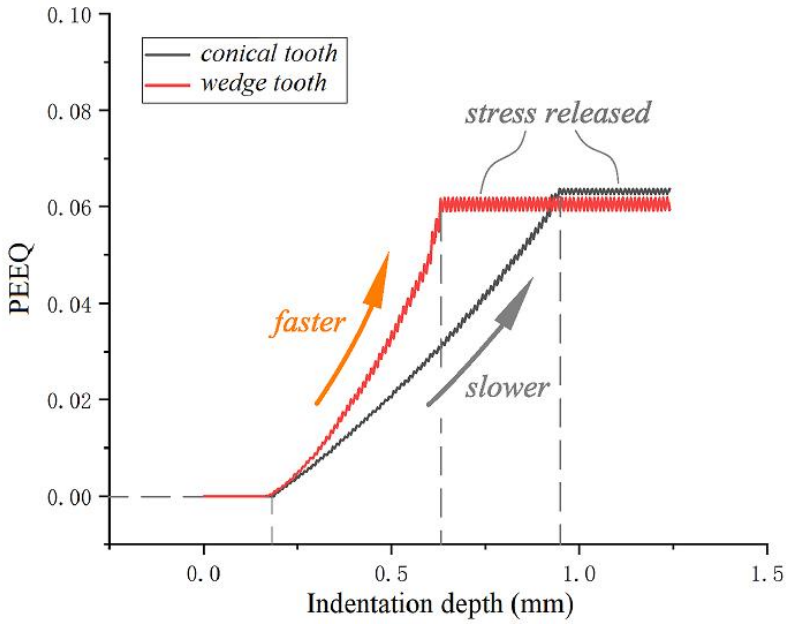

Figure 30. Variation of PEEQ in intermediate area between indenters.

4.5. Discussion on the Simulation Results

According to the simulation results, it was found that: first, the unbroken intermediate area in the indentation of wedge teeth was much smaller than the conical teeth, which was beneficial to realizing the volumetric fracture between the teeth; second, the plastic strain on the intermediate area between the wedge teeth was more concentrated and increased faster than that between the conical teeth, thus the intermediate area could be removed more easily even though the forces exerted on the teeth were the same; third, the rock material beneath the wedge teeth was removed earlier than the material beneath the conical teeth and, accordingly, the rock in the intermediate area between the wedge teeth would be damaged sooner than that between the conical teeth.

By comparing the damage performance of wedge teeth and conical teeth in the simulation, it was found that the wedge tooth can penetrate rock more easily because the

narrow tooth crown can generate larger specific stress in the rock, and the wedge tooth can generate more volumetric rock breakage than the conical tooth because the damaged rock area of the wedge tooth is concentrated in the shallow area of the rock, whereas the damage area of the conical tooth tends to extend deeper. Although the wedge tooth is narrower than the conical tooth in the breadth direction, the damage area of the wedge tooth in the breadth direction is almost equal to that of the conical tooth. On the other hand, because the damage area of the wedge tooth in the length direction is apparently larger than the conical tooth, the damage area of the wedge tooth is generally larger than the conical tooth.

5. Conclusions

First, the load-displacement curves and rock damaging status achieved in the experiment show that the load requirement of the wedge tooth is lower than the conical tooth, and that the wedge tooth is more efficient in fracturing and damaging rock, especially limestone.

Second, indenters or teeth with different crowns break the rock with the same mechanism: a compacted core will first be formed in the indentation process, and the damage inside the rock results from the occurrence of a compacted core and the wedging force generated by the compacted core. Once the wedging or pressing force reaches the limit of the rock strength, the rock around the core will be damaged.

Third, the original internal defects of the rock has little effect on crack propagation direction under the indentation of the wedge tooth because the narrow and long tooth crown of the wedge tooth forces the cracks to grow along the length direction of the wedge tooth. However, for the conical tooth with its axisymmetric crown, the crack propagation direction is obviously affected by the original internal defects of the rock, thus the cracks under the indentation of conical tooth appear to propagate in random directions.

Four, between the damage performance of the wedge tooth and the conical tooth, it was found that the wedge tooth can penetrate in the rock more easily than the conical tooth because the narrow tooth crown can generate larger specific stress in the rock and is able to generate more volumetric rock breakage.

Moreover, although the wedge tooth is narrower than the conical tooth in the breadth direction, numerical simulation has proven that the damage area of the wedge tooth in the breadth direction is almost equal to that of the conical tooth. On the other hand, because the damage area of the wedge tooth in the length direction is apparently larger than that of the conical tooth, the total damage area of the wedge tooth is larger than that of the conical tooth.

Drilling efficiency is one of the most important factors affecting drill bit performance in oil and gas drilling. The experiment and simulation results in this paper have proved the advantages of the wedge tooth in rock fracturing and damaging, and proper application of the wedge tooth in the drill bit is expected to improve the overall performance of the bit, thus providing technical support for development and optimization of the drill bits applied in oil and gas drilling.

Author Contributions: Conceptualization, Q.Q. and Y.Y.; methodology, S.N.; software, X.C.; validation, Q.Q. and Y.Y.; formal analysis, L.C.; investigation, S.N.; resources, Q.Q.; data curation, S.N.; writing—original draft preparation, Q.Q.; writing—review and editing, Y.Y.; visualization, S.N.; supervision, Y.Y.; project administration, Y.Y.; funding acquisition, S.N. All authors have read and agreed to the published version of the manuscript.

Funding: Financial support for this work was provided by the Sichuan Natural Science Foundation Project (Grant No. 22NSFSC3078) and Postdoctoral Science Foundation of China (Grant No. 2021M693909).

Institutional Review Board Statement: Not applicable.

Informed Consent Statement: Not applicable.

Data Availability Statement: The original contributions presented in the study are included in the article, and further inquiries can be directed to the corresponding author.

Conflicts of Interest: The authors declare no conflict of interest.

References

1. Zhu, X.H.; Liu, W.J. Rock-breaking Process and Rock Degradation of Rock under Wedge-tooth Penetrating. *J. China Univ. Pet. (Ed. Nat. Sci.)* **2017**, *41*, 90–95.
2. Niu, S.W.; Zheng, H.; Yang, Y.; Chen, L. Experimental study on the rock-breaking mechanism of disc-like hybrid bit. *J. Pet. Sci. Eng.* **2018**, *161*, 541–550. [CrossRef]
3. Chen, L.H.; Labuz, J.F. Indentation of rock by wedge shaped tools. *Int. J. Rock Mech. Min. Sci.* **2006**, *43*, 1023–1033. [CrossRef]
4. Hood, M.C.; Roxborough, F.F. Rock breakage: Mechanical. In *SME Mining Engineering Handbook*; Society for Mining, Metallurgy & Exploration: Englewood, CO, USA, 1992; Volume 1, pp. 680–721.
5. Yin, L.J.; Gong, Q.M.; Ma, H.S.; Zhao, J.; Zhao, X.B. Use of indentation tests to study the influence of confining stress on rock fragmentation by a TBM cutter. *Int. J. Rock Mech. Min. Sci.* **2014**, *72*, 261–276. [CrossRef]
6. Liu, H.Y.; Kou, S.Q.; Lindqvist, P.A. Numerical Studies on Bit-Rock Fragmentation Mechanisms. *Int. J. Geomech.* **2008**, *8*, 45–67. [CrossRef]
7. Liu, H.Y.; Kou, S.Q.; Lindqvist, P.A.; Tang, C.A. Numerical simulation of the rock fragmentation process induced by indenters. *Int. J. Rock Mech. Min. Sci.* **2002**, *39*, 491–505. [CrossRef]
8. Kou, S.Q.; Liu, H.Y.; Lindqvist, P.A.; Tang, C.A. Rock fragmentation mechanisms induced by a drill bit. *Int. J. Rock Mech. Min. Sci.* **2004**, *41*, 527–532. [CrossRef]
9. Souissi, S.; Miled, K.; Hamdi, E.; Sellami, H. Numerical modeling of rock damage during indentation process with reference to hard rock drilling. *Int. J. Geomech.* **2017**, *17*, 04017002. [CrossRef]
10. Saksala, T.; Fourmeau, M.; Kane, P.A.; Hokka, M. 3D finite elements modelling of percussive rock drilling: Estimation of rate of penetration based on multiple impact simulations with a commercial drill bit. *Comput. Geotech.* **2018**, *99*, 55–63. [CrossRef]
11. Saksala, T.; Gomon, D.; Hokka, M.; Kuokkala, V.T. Numerical and experimental study of percussive drilling with a triple-button bit on Kuru granite. *Int. J. Impact Eng.* **2014**, *72*, 56–66. [CrossRef]
12. Shariati, H.; Saadati, M.; Bouterf, A.; Weeddfelt, K.; Larsson, P.L.; Hild, F. On the Inelastic Mechanical Behavior of Granite: Study Based on Quasi-oedometric and Indentation Tests. *Rock Mech. Rock Eng.* **2019**, *52*, 645–657. [CrossRef]
13. Saadati, M.; Forquin, P.; Weddfelt, K.; Larsson, P.L.; Hild, F. Granite rock fragmentation at percussive drilling-experimental and numerical investigation. *Int. J. Numer. Anal. Methods Geomech.* **2013**, *38*, 828–843. [CrossRef]
14. Zhang, F.; Huang, H.; Vajdova, V. Discrete element modeling of sphere indentation in rocks. In Proceedings of the 45th US Rock Mechanics/Geomechanics Symposium, San Francisco, CA, USA, 26–29 June 2011.
15. Shi, X.C.; Meng, Y.; Li, G.; Li, J.; Zhao, X. The influence of load speed on the rock-breaking process of single tooth indenting. *Pet. Drill. Tech.* **2010**, *38*, 3.
16. Maurer, W.C. Bit-tooth penetration under simulated borehole conditions. *JPT* **1965**, *17*, 1433–1442. [CrossRef]
17. Qi, L.; Liu, Q.; Pan, Y.; Peng, X.; Demg, P.; Huang, K. Experimental study on rock indentation using infrared thermography and acoustic emission techniques. *J. Geophys. Eng.* **2018**, *15*, 1864–1877.
18. Buljak, V.; Cocchetti, G.; Cornaggia, A.; Maier, G. Assessment of residual stresses and mechanical characterization of materials by "hole drilling" and indentation tests combined and by inverse analysis. *Mech. Res. Commun.* **2015**, *68*, 18–24. [CrossRef]
19. Kalyan, B.; Murthy, C.; Choudhary, R. Rock indentation indices as criteria in rock excavation technology–A critical review. *Procedia Earth Planet. Sci.* **2015**, *11*, 149–158. [CrossRef]
20. Kahraman, S.; Fener, M.; Kozman, E. Predicting the compressive and tensile strength of rocks from indentation hardness index. *J. South. Afr. Inst. Min. Metall.* **2012**, *112*, 331–339.
21. Haftani, M.; Bohloli, B.; Nouri, A.; Javan, M.; Moosavi, M. Size effect in strength assessment by indentation testing on rock fragments. *Int. J. Rock Mech. Min. Sci.* **2014**, *65*, 141–148. [CrossRef]
22. Tan, Q.; Zhang, K.; Zhou, Z.; Xia, Y. Experiment and simulation on rock cracking under spherical tooth pressing. *J. Rock Mech. Geotech. Eng.* **2010**, *29*, 163–169.
23. Tan, Q.; Li, J.; Xia, Y.; Xu, Z.; Zhu, Y.; Zhang, J. Numerical simulation on rock-breaking process of disc roller. *Rock Soil Mech.* **2013**, *34*, 2707–2714.
24. Zhang, H.; Song, H.; Kang, Y.; Huang, G.; Qu, C. Experimental analysis on deformation evolution and crack propagation of rock under cyclic indentation. *Rock Mech. Rock Eng.* **2013**, *46*, 1053–1059. [CrossRef]
25. Carpinteri, A.; Invernizzi, S. Numerical analysis of the cutting interaction between indenters acting on disordered materials. *Int. J. Fract.* **2005**, *131*, 143–154. [CrossRef]
26. Kou, S.Q.; Huang, Y.; Tan, X.C.; Lindqvist, P.A. Identification of the governing parameters related to rock indentation depth by using similarity analysis. *Eng. Geol.* **1998**, *49*, 261–269. [CrossRef]
27. Kou, S.Q. Some Basic Problems in Rock Breakage by Blasting and by Indentation. Ph.D. Thesis, Luleå Tekniska Universitet, Luleå, Sweden, 1995.

28. Haeri, H.; Sarfarazi, V.; Fatehi Marji, M. Experimental and numerical investigation of uniaxial compression failure in rock-like specimens with L-shaped nonpersistent cracks. *Iran. J. Sci. Technol. Trans. Civ. Eng.* **2021**, *45*, 2555–2575. [CrossRef]
29. Xi, D.; Xu, S. *Rock Physics and Constitutive Theory*; Press USCT: Hefei, China, 2016; pp. 18–24.
30. Zhang, C. Research on Rock-Breaking Mechanism and Design Theory of the Cross-Cutting PDC Bit. Doctoral dissertation, China University of Petroleum, Beijing, China, 2018; pp. 35–37.
31. Fei, K.; Zhang, J.W. *The application of ABAQUS in geotechnical engineering*; China Water & Power Press: Beijing, China, 2013; pp. 61–81.
32. Zirpoli, A.; Maier, G.; Novati, G.; Garbowski, T. Dilatometric tests combined with computer simulations and parameter identification for in-depth diagnostic analysis of concrete dams. In *Life-Cycle Civil Engineering*; CRC Press: Boca Raton, FL, USA, 2008; pp. 279–284.
33. Buljak, V.; Baivier-Romero, S.; Kallel, A. Calibration of Drucker–Prager Cap Constitutive Model for Ceramic Powder Compaction through Inverse Analysis. *Materials* **2021**, *14*, 4044. [CrossRef] [PubMed]
34. Buljak, V.; Cocchetti, G.; Cornaggia, A.; Garbowski, T.; Maier, G.; Novati, G. Materials mechanical characterizations and structural diagnoses by inverse analyses. In *Handbook of Damage Mechanics*; Voyiadjis, G., Ed.; Springer Nature: New York, NY, USA, 2015; pp. 619–642.